NANO LETTERS

pubs.acs.org/NanoLett Letter

Gate-Controlled Magnetic Phase Transition in a van der Waals Magnet Fe_5GeTe_2

Cheng Tan,[†] Wen-Qiang Xie,[†] Guolin Zheng,* Nuriyah Aloufi, Sultan Albarakati, Meri Algarni, Junbo Li, James Partridge, Dimitrie Culcer, Xiaolin Wang, Jia Bao Yi, Mingliang Tian, Yimin Xiong, Yu-Jun Zhao,* and Lan Wang*

Cite This: *Nano Lett.* 2021, 21, 5599−5605 Read Online

ACCESS | Metrics & More | Article Recommendations | Supporting Information

Downloaded via SOUTH CHINA UNIV OF TECHNOLOGY on September 28, 2021 at 01:49:01 (UTC).
See https://pubs.acs.org/sharingguidelines for options on how to legitimately share published articles.

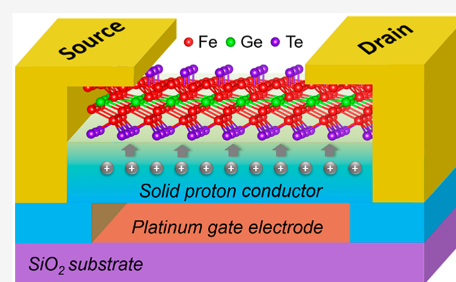

ABSTRACT: Magnetic van der Waals (vdW) materials are poised to enable all-electrical control of magnetism in the two-dimensional limit. However, tuning the magnetic ground state in vdW itinerant ferromagnets by voltage-induced charge doping remains a significant challenge, due to the extremely large carrier densities in these materials. Here, by cleaving the vdW itinerant ferromagnet Fe_5GeTe_2 (F5GT) into 5.4 nm (around two unit cells), we find that the ferromagnetism (FM) in F5GT can be substantially tuned by the thickness. Moreover, by utilizing a solid protonic gate, an electron doping concentration of above 10^{21} cm^{-3} has been exhibited in F5GT nanosheets. Such a high carrier accumulation exceeds that possible in widely used electric double-layer transistors (EDLTs) and surpasses the intrinsic carrier density of F5GT. Importantly, it is accompanied by a magnetic phase transition from FM to antiferromagnetism (AFM). The realization of an antiferromagnetic phase in nanosheet F5GT suggests the promise of applications in high-temperature antiferromagnetic vdW devices and heterostructures.

KEYWORDS: *Fe_5GeTe_2, van der Waals ferromagnetism, magnetic phase transition, solid protonic gating*

Control of magnetism and magnetic properties by voltage is vital to modern low-energy nanoelectronic devices.[1−3] In traditional FM metals, tuning of magnetism by voltage-induced charge doping is limited to the surface,[4] due to the strong electric-field screening effect in FM metals. The emergence of vdW magnetic materials[5−7] has greatly expedited the development of vdW spintronic devices[8−14] and, thanks to the extreme large surface-to-bulk ratio in atomically thin layers, provided an unrivalled opportunity to manipulate magnetism in the two-dimensional (2D) limit by all-electrical means.[7,15−18] However, voltage-control of the magnetic ground state in vdW itinerant FMs has remained elusive. This is because the high carrier concentrations in vdW itinerant FMs exceed those in any traditional field-effect transistors or widely used electric double-layer transistors (EDLTs).[19]

Here, we report a systematic investigation of the anomalous Hall effect in vdW itinerant FM Fe_5GeTe_2(F5GT). Both the coercivity and the critical temperature of the ferrimagnetic transition of Fe^1 sites depend strongly on the thickness of the F5GT. Furthermore, we fabricate a solid proton field-effect transistor (SP-FET) and demonstrate that an electron doping concentration of above 10^{21} cm^{-3} (or 10^{16} cm^{-2} in 2D) can be achieved with just a few volts applied to the gate. This is an order of magnitude increase over doping concentrations achievable in EDLTs.[19] In the F5GT nanosheets, the high gate voltage-induced doping suppresses the hysteresis of the FM state, leading to a magnetic phase transition from FM to AFM. This ability to control the magnetic phase in F5GT via gate voltages suggests the possibility of antiferromagnetic spintronic devices that operate at high temperatures and a new pathway in the search for vdW itinerant AFMs.

F5GT is a newly synthesized vdW ferromagnet[20−24] which is noteworthy due to its high Curie temperature (T_c). This T_c approaches room temperature and exceeds the Curie temperature of up to 230 K exhibited by the widely investigated itinerant vdW FM Fe_3GeTe_2 (FGT).[7,25−28] Figure 1a illustrates a schematic diagram of the Fe_5GeTe_2 crystal structure projected along the [100] direction. Like FGT, the F5GT crystal is formed from thicker Fe−Ge slabs sandwiched by Te layers. The crystal structure of F5GT has a space group $R\bar{3}m$ with lattice parameters a = 4.04 Å and c = 29.19 Å.[20] In each unit cell, there are 3 Fe sites, and the Fe^1 site is regarded as a split site located either above or below the Ge site, leading to the complex crystal structure. Figure 1b shows optical and atomic force microscope images of an ultrathin F5GT

Received: March 18, 2021
Revised: June 17, 2021
Published: June 21, 2021

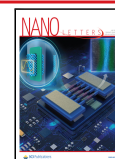

ACS Publications © 2021 American Chemical Society

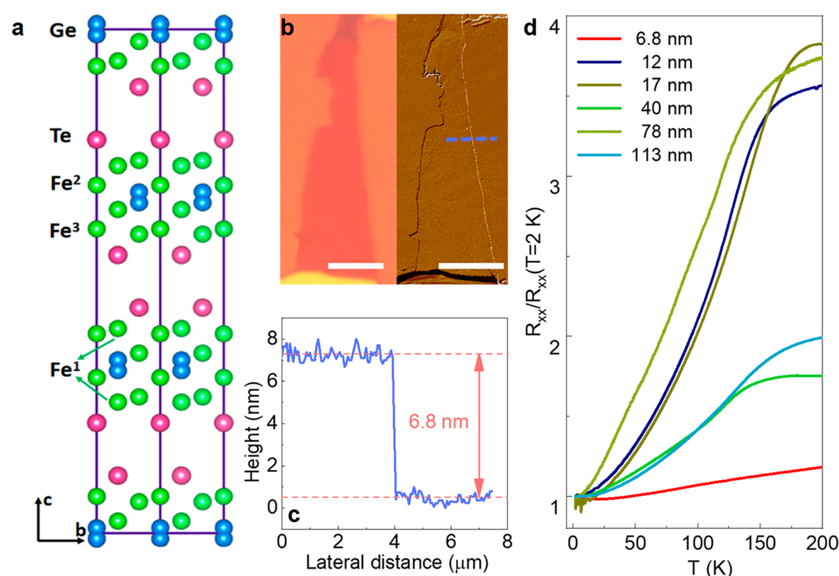

Figure 1. Crystal structure and initial characterization of Fe_5GeTe_2. (a) Schematic diagram of the F5GT crystal structure viewed along the *a*-axis. (b) Optical and atomic force microscope images of a thin F5GT nanosheet. The white scale bars represent 5 μm. (c) Cross-sectional profile of the F5GT flake along the dashed line in part b. (d) Temperature-dependent longitudinal resistances of F5GT devices with various thicknesses. Resistances are normalized to their values at T = 2 K.

nanosheet supported on a SiO_2 substrate. Figure 1c illustrates the lateral distance-dependent height (corresponding to the dashed blue line in Figure 1b) of a thin F5GT nanosheet, indicating a thickness of 6.8 nm. The normalized resistance vs temperature (RT) curves of F5GT devices with various thicknesses are shown in Figure 1d. In samples with thicknesses exceeding 6.8 nm, the RT curves exhibit a kink around $T \approx 145$ K. This resistance anomaly is attributed to the gradual magnetic transition of the Fe^1 site with decreasing temperature,[20] as discussed later. A small response near 115 K is observed in the magnetization data collected from the bulk crystal at 1 T (Figure S1a), which is also indicative of a first-order transition of the magneto-structure.[20,21]

Figure 2a illustrates the magnetic field-dependent anomalous Hall resistivity (ρ_{xy}) of F5GT nanosheets with different thicknesses. All measurements were performed with the magnetic field oriented perpendicular to the planes of the nanosheets. The 113 nm nanosheet exhibits a hard magnetic property with two magnetic phases and a small coercive field (H_c) of 65.5 mT. These attributes agree well with the magnetic measurements taken from the single crystal (Figure S1). Reducing the thickness from 113 to 40 nm, $\rho_{xy}(0\ \mathrm{T})/\rho_{xy}^{\mathrm{SAT}}$ (with ρ_{xy}^{SAT} being the saturated anomalous Hall resistivity) increases from 0.24 to 0.73, and the coercive field correspondingly increases to 93.8 mT in the 40 nm thick nanosheet. Furthermore, the magnetic loops from the samples of thickness 17 and 12 nm exhibit larger H_c and are nearly square-shaped with $\rho_{xy}(0\ \mathrm{T})/\rho_{xy}^{\mathrm{SAT}}$ values approaching unity. Further lowering the thickness to 5.4 nm results in a single, hard magnetic phase with a large H_c of 1.7 T and a $\rho_{xy}(0\ \mathrm{T})/\rho_{xy}^{\mathrm{SAT}}$ ratio of 1. The larger $\rho_{xy}(0\ \mathrm{T})/\rho_{xy}^{\mathrm{SAT}}$ ratios indicate the magnetic moments align perpendicular to the plane of the nanosheet at the remanence point in thinner F5GT nanosheets, implying a strong magnetic perpendicular anisotropy. Interestingly, few-layer F5GT nanoflakes exhibit a much larger (around 4 times) coercivity than FGT nanoflakes of similar thicknesses. In the absence of defects, the coercivity is mainly determined by the magnetic anisotropic energy (MAE).

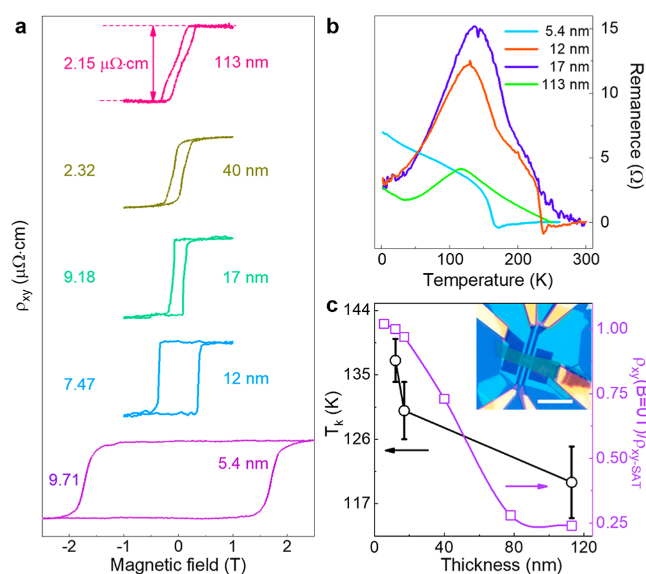

Figure 2. Anomalous Hall effect measurements performed on Fe_5GeTe_2 devices of various thicknesses. (a) $\rho_{xy}(B)$ for F5GT nanosheets of various thicknesses at 2 K. (b) Temperature-dependent remanence curves from devices with thicknesses ranging from 5.4 to 113 nm. (c) Thickness-dependent $\rho_{xy}(B = 0\ \mathrm{T})/\rho_{xy}^{\mathrm{SAT}}$ (at T = 2 K) and T_k. Inset displays the optical image of a thin F5GT device covered with a h-BN layer. The white scale bar represents 5 μm.

However, the MAE of F5GT is much smaller than that of FGT nanoflakes (see Table S3), revealing that the pinning effect induced by defects might play a pivotal role in the coercivity mechanism, given that F5GT usually has much more Fe-deficiency-induced defects in a comparison with FGT. While the theoretically calculated interlayer depinning field is only ~3.7 kOe (see Supporting Information), this is still considerably smaller than the measured coercivity (~20 kOe) in few-layer F5GT. Therefore, the defect-induced intralayer pinning effect possibly contributes to the large coercivity in

https://doi.org/10.1021/acs.nanolett.1c01108
Nano Lett. 2021, 21, 5599−5605

few-layer F5GT. In thicker F5GT nanoflakes, the chance of domain expansion along the interlayer direction can be largely enhanced. Accordingly, the interlayer depinning field and the MAE will gradually dominate the mechanism of coercivity and result in much smaller coercivity in thicker F5GT.

Figure 2b shows the temperature-dependent remanence of F5GT nanosheets with different thicknesses. In the nanosheets with a thickness above 5.4 nm, the remanence first increases with decreasing temperature and reaches a maximum at around 120−150 K, before declining sharply. This behavior indicates that the phase in thicker F5GT nanosheets is ferrimagnetic rather than ferromagnetic.[20−22] However, for the 5.4 nm F5GT device, the lack of the "peak" in the temperature-dependent remanence curve indicates that the first-order magnetic transition of the Fe^1 sites disappears, and the curve shows a typical ferromagnetic behavior. Note that the remanence of the 5.4 nm thick F5GT nanosheet decreases to zero at around 220 K, revealing a lower T_c. This lower T_c may result from weaker interlayer magnetic coupling due to the reduced number of layers, as reported to be the case in other vdW magnets.[5,7,26] As discussed above (Figure S1a), the magnetic transition on the Fe^1 site results in a first-order transition on the temperature-dependent magnetization curve of the bulk crystal. In F5GT nanosheets, the temperature-dependent magnetization curves correspond to the temperature-dependent remanence curves, and we define the temperature at which the remanence is at a maximum as the critical temperature (T_k) of the ferrimagnetic transition on the Fe^1 sites. Figure 2c shows the thickness-dependent $\rho_{xy}(0\ \mathrm{T})/\rho_{xy}^{\mathrm{SAT}}$ and T_k. T_k gradually increases with decreasing thickness and eventually disappears in the 5.4 nm thick nanosheet. The abrupt disappearance of a ferrimagnetic transition of Fe^1 sites in the 5.4 nm thick F5GT reveals a magnetic phase transition between the thicknesses of 12 and 5.4 nm, again possibly due to the increased intralayer pinning effect discussed above.

In vdW materials, controlling the magnetism by the application of voltage would enable a greater number of applications in spintronics and memory devices. For vdW itinerant magnets, however, conventional field-effect transistors or EDLTs[19] are insufficient for electrical control of the magnetic order, due to their limited capacities. To date, protonic intercalation induced by a protonic gate[29] has proved effective in tuning the magnetism and interlayer coupling in vdW itinerant FM FGT. Using the same protonic gate technique, as illustrated in Figure 3a, we fabricate a SP-FET and find that the FM in F5GT nanosheets can be significantly modulated. Figure 3b shows the magnetic field-dependent anomalous Hall resistivity ρ_{xy} at various gate voltages in the 40 nm thick F5GT at 2 K. In the pristine nanosheet, the hysteresis loop shows a large ρ_{AHE} value, with ρ_{AHE} defined by $\rho_{\mathrm{AHE}} = |\rho_{xy}(1\ T) - \rho_{xy}(-1\ T)|$. Sweeping the voltage from 0 V to V_g = −3.1 V and −3.6 V, we find the ρ_{AHE} decreases accordingly. The anomalous Hall resistivity can usually be written as $\rho_{xy} = R_0H + \rho_{xy}^{A} = R_0H + R_sM_z$, where M_z represents the magnetization.[30] As the normal Hall section R_0H is small compared with the whole anomalous Hall resistance, the hysteresis loop here is proportional to the magnetization loop, so the decrease of ρ_{xy} indicates a decrease in the magnetization. If the magnitude of the gate voltage is increased, the anomalous Hall resistivities are further suppressed and exhibit a sign reversal at −4.2 and −4.5 V, as discussed later. At V_g = −5 V, the anomalous Hall loop eventually disappears, implying the possibility of a magnetic phase transition. Note that the

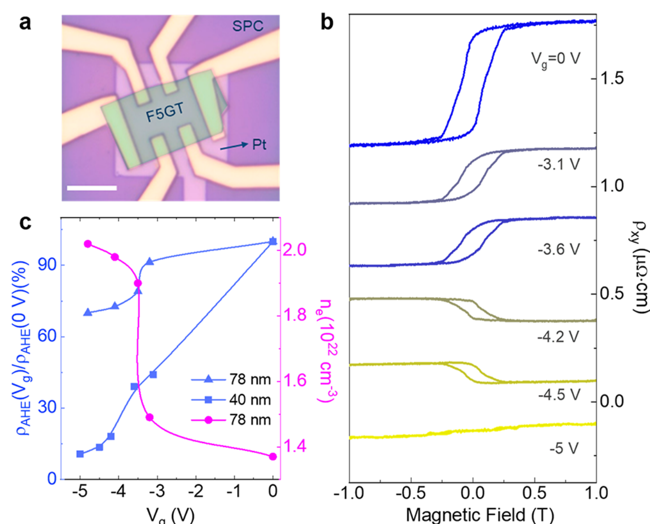

Figure 3. Protonic gating modulation of the 40 nm Fe_5GeTe_2 nanosheet. (a) Schematic diagram of a F5GT SP-FET, where an F5GT flake lies on the solid proton conductor (SPC). The scale bar represents 10 μm. (b) $\rho_{xy}(B)$ loops at various gating voltages on the 40 nm thick F5GT device. (c) Gate voltage-dependent carrier densities and anomalous Hall ratios of the 40 and 78 nm thick F5GT nanosheets. The definition of the ρ_{AHE} is the same as that given in Figure 2a.

transport properties of F5GT nanoflakes are almost unchanged under the positive voltages and the gate-induced proton intercalation/deintercalation process mainly occurs in the negative voltage range.

Note that the anomalous Hall resistivities exhibited by nanosheets thinner than 40 nm are nearly "flat" at high magnetic fields. In order to qualitatively determine the doping concentrations during the gating process, we tested more samples with different thicknesses (Figure S3). In a 78 nm thick nanosheet, we found that negative gate voltages led to electron-type doping (Figure S3a) which suppressed the anomalous Hall resistivity. A similar suppression of anomalous Hall resistivity has also been identified in other samples at negative gate voltages, indicating the same n-type doping at negative gate voltages. We can rule out the possibility of the magnetic anisotropy changing from out-of-plane to in-plane, because there is no magnetic hysteresis loop at V_g = −5 V. An in-plane magnetization should be rotated to the perpendicular direction gradually under an increasing perpendicular magnetic field, and this is not shown in our results. Therefore, the absence of a hysteresis loop at V_g = −5 V is attributed to the formation of an AFM state. Figure 3c shows the V_g-dependent carrier density of a 78 nm thick nanosheet as well as the $\rho_{\mathrm{AHE}}(V_g)/\rho_{\mathrm{AH}}(0\ V)$ of 40 and 78 nm thick nanosheets, respectively. Sweeping the voltage V_g from 0 to −5 V, $\rho_{\mathrm{AHE}}(V_g)/\rho_{\mathrm{AHE}}(0\ V)$ values in both the 40 and 78 nm thick nanosheets decrease while the electron density in the 78 nm thick nanosheet increases by 0.8 × 10^{22} cm^{-3}. As discussed above, since $\rho_{\mathrm{AHE}}(V_g)/\rho_{\mathrm{AHE}}(0\ V)$ of the 40 nm thick nanosheet exhibits a similar tendency under negative gate voltages, we speculate that an electron doping concentration of above 10^{21} cm^{-3} could totally suppress ferromagnetism and give rise to a magnetic phase transition from FM to AFM in F5GT nanosheets. Generally, the maximal carrier accumulation in widely used EDLTs[19] is less than 10^{15} cm^{-2}, which is at least one order smaller than present solid protonic gates (above 10^{16}

https://doi.org/10.1021/acs.nanolett.1c01108
Nano Lett. 2021, 21, 5599−5605

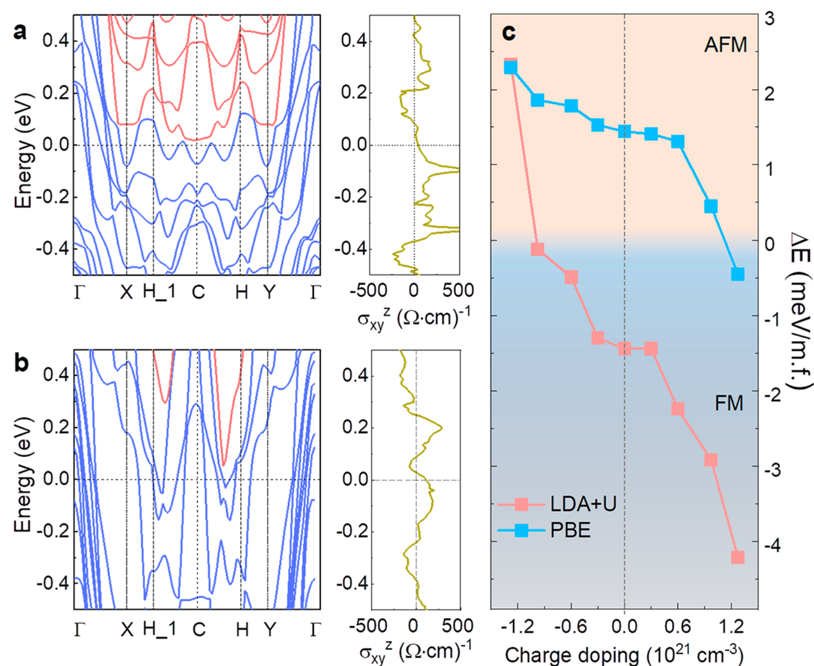

Figure 4. Theoretical calculation. (a) PBE band structure with corresponding Hall conductivity in F5GT. (b) LDA+U band structure with corresponding Hall conductivity in F5GT. In parts a and b, the red lines indicate the energy bands fully located above Fermi level, while blue lines indicate the other bands. (c) Evolution of energy difference between FM and AFM (ΔE) with charge doping under LDA+U and PBE functionals. The ochre region indicates AFM coupling, while the blue region indicates FM coupling.

cm^{-2} in 2D). The extremely high electron doping concentrations observed in F5GT can be ascribed to the high mobility of protons which are easily intercalated into vdW materials under modest gate voltages. This leads to a dramatic change of carrier density within the F5GT. Recent experiments have revealed that the cobalt substitution can change the intralayer local configuration and interlayer stacking configuration of F5GT (or Fe_4GeTe_2[31]) and result in AFM states.[32−34] In addition, the gate-controlled charge doping here mainly changes the magnetic interaction in F5GT by affecting the interlayer coupling energy (see Figures S6 and S7) and results in a possible *in situ* magnetic phase transition in nanodevices, potentially enabling greater applications in vdW spintronics.

As mentioned above, the anomalous Hall loops exhibit sign reversal during the gate process (at $V_g = -4.2$ V and -4.5 V); this reversal in the hysteresis loops indicates the reversal of $\rho_{xy}^A = R_s M_z$. The latter could merely be ascribed to the flip of the total magnetization M_z due to the change of carrier type. However, since there is no experimental evidence of sign change in the Hall slope around $V_g = -4.5$ V, this change in ρ_{xy}^A cannot be simply attributed to a change of carrier type. To obtain more insight, we calculated the anomalous Hall conductivity in terms of Berry curvature.[30,35] Band structures and relativistic anomalous Hall conductivity (σ_{xy}^z component) based on density functional theory (DFT) calculations with PBE (Perdew−Burke−Ernzerhof) and LDA+U (local density approximation plus Hubbard U) functionals,[36−39] with consideration of spin−orbit coupling (SOC), are presented in Figure 4a,b, respectively. Hartree−Fock band structures[40] without SOC are also shown in Figure S5. Despite the different theoretical functionals employed, they all reveal that an electron doping treatment of the system can indeed lead to a reversal of Hall conductivity σ_{xy}^z. This qualitatively agrees with the reversed anomalous Hall resistivity at $V_g = -4.2$ and -4.5 V, indicating the intrinsic topological nature of the effect.

To further assess the experimental results above, additional DFT calculations with PBE and LDA+U functionals were carried out. Figure 4c shows the doping-dependent energy difference between FM and AFM. Here, the ΔE is defined as $\Delta E = E_{FM} - E_{AFM}$, where E_{AFM} and E_{FM} represent the energy of antiferromagnetic and ferromagnetic F5GT, respectively. Both PBE and LDA+U functionals exhibit a doping-dependent ΔE. Moreover, ΔE values of LDA+U and PBE are only −1.42 and 1.45 meV, respectively. This may explain the highly tunable hysteresis loop as well as the magnetic order in F5GT under various gate voltages. We first rule out the possibility of a paramagnetic phase in electron-doped F5GT. This is because the pristine F5GT nanosheets have a high Curie temperature ($T_C \geq 250$ *K*, Figure S2), indicating a large energy gap (>20 meV) between the FM state and the paramagnetic state at 2 K, which is much larger than ΔE calculated from both LDA+U and PBE methods. In pristine F5GT, ΔE should be negative due to its FM ground state. As shown in Figure 4c, electron doping applied in both PBE and LDA+U functionals can narrow the energy discrepancy between FM and AFM and eventually lead to a positive ΔE, or an AFM ground state. This tunable magnetism for F5GT is mainly due to the evolution of interlayer coupling under various charge dopings (Figure S6a). On the other hand, the intralayer magnetism almost stays unchanged with the doping (Figure S6b). The doping amount corresponds with the experimental observation qualitatively such that the hysteresis loops are gradually suppressed and eventually disappear when electron doping exceeds 10^{21} cm^{-3}. The charge density difference in Figure S7 shows that the whole layer is affected by electron doping as the charge accumulation regions spread over the atomic volume.

In conclusion, we have studied the anomalous Hall effect in a vdW itinerant ferromagnet F5GT. This study was performed with different thicknesses and gating voltages to show that the magnetic ground state in F5GT can be tuned *in situ* by a gate

https://doi.org/10.1021/acs.nanolett.1c01108
Nano Lett. 2021, 21, 5599−5605

voltage. An electron doping concentration of above 10^{21} cm^{-3} induced in F5GT by a protonic gate can trigger a magnetic phase transition from FM to AFM. Theoretical calculations based on DFT support the experimental observations and demonstrate that the F5GT can be modulated from an FM state to an AFM ground state by electron doping. Realizing an AFM phase in vdW FM F5GT nanosheets by protonic gating may constitute an important step toward vdW antiferromagnetic devices and heterostructures that operate at high temperatures.

■ ASSOCIATED CONTENT

Supporting Information

The Supporting Information is available free of charge at https://pubs.acs.org/doi/10.1021/acs.nanolett.1c01108.

> Methods, magnetic measurements, detailed hysteresis behaviors of 113 and 6.8 nm F5GT devices, protonic gating modulation of other 3 devices at 2 K, angle-dependent anomalous Hall measurement of 6.8 and 17 nm devices, basic properties of F5GT calculated by density functional theory with various functionals, density functional theory calculations of ΔE based on thickness of F5GT, Hartree–Fock band structures without SOC and corresponding Hall conductivity, calculated interlayer and intralayer magnetic couplings of F5GT, charge density difference of electron doping F5GT, coercivity in few-layer F5GT and FGT, and decrease of coercivity with the increase of thickness in FGT and F5GT nanoflakes (PDF)

■ AUTHOR INFORMATION

Corresponding Authors

Guolin Zheng – *School of Science, RMIT University, Melbourne, Victoria 3001, Australia*; Email: guolin.zheng@rmit.edu.au

Yu-Jun Zhao – *Department of Physics, South China University of Technology, Guangzhou 510640, China*; orcid.org/0000-0002-6923-1099; Email: zhaoyj@scut.edu.cn

Lan Wang – *School of Science, RMIT University, Melbourne, Victoria 3001, Australia*; orcid.org/0000-0001-7124-2718; Email: lan.wang@rmit.edu.au

Authors

Cheng Tan – *School of Science, RMIT University, Melbourne, Victoria 3001, Australia*

Wen-Qiang Xie – *Department of Physics, South China University of Technology, Guangzhou 510640, China*

Nuriyah Aloufi – *School of Science, RMIT University, Melbourne, Victoria 3001, Australia*

Sultan Albarakati – *School of Science, RMIT University, Melbourne, Victoria 3001, Australia*

Meri Algarni – *School of Science, RMIT University, Melbourne, Victoria 3001, Australia*

Junbo Li – *Anhui Province Key Laboratory of Condensed Matter Physics at Extreme Conditions, High Magnetic Field Laboratory, Chinese Academy of Sciences (CAS), Hefei 230031, Anhui, China*

James Partridge – *School of Science, RMIT University, Melbourne, Victoria 3001, Australia*

Dimitrie Culcer – *School of Physics and ARC Centre of Excellence in Future Low-Energy Electronics Technologies, UNSW Node, University of New South Wales, Sydney, New South Wales 2052, Australia*

Xiaolin Wang – *Institute for Superconducting & Electronic Materials, Australian Institute of Innovative Materials and ARC Centre for Future Low-Energy Electronics Technologies (FLEET), University of Wollongong, Wollongong, New South Wales 2500, Australia*; orcid.org/0000-0003-4150-0848

Jia Bao Yi – *Global Innovative Center for Advanced Nanomaterials, School of Engineering, University of Newcastle, Callaghan, New South Wales 2308, Australia*; orcid.org/0000-0001-5299-9897

Mingliang Tian – *Anhui Province Key Laboratory of Condensed Matter Physics at Extreme Conditions, High Magnetic Field Laboratory, Chinese Academy of Sciences (CAS), Hefei 230031, Anhui, China; Department of Physics, School of Physics and Materials Science, Anhui University, Hefei 230601, Anhui, China; Collaborative Innovation Center of Advanced Microstructures, Nanjing University, Nanjing 210093, China*; orcid.org/0000-0002-0870-995X

Yimin Xiong – *Anhui Province Key Laboratory of Condensed Matter Physics at Extreme Conditions, High Magnetic Field Laboratory, Chinese Academy of Sciences (CAS), Hefei 230031, Anhui, China*

Complete contact information is available at: https://pubs.acs.org/10.1021/acs.nanolett.1c01108

Author Contributions

†C.T. and W.-Q.X contributed equally. G.Z. and L.W. conceived and designed the research. C.T., S.A. and M.A. fabricated the solid proton gate. C.T., N.A. and G.Z. did the device fabrication. C.T. and G.Z. performed the electron transport measurements. W.-Q. X. and Y.-J. Z. did the theoretical calculation. J.L. and Y.X. synthesized the material. X.W., J.B.Y., M.T., Y.X., D.C., Y.-J Z. and L.W. did the data analysis and modeling. C.T., W.-Q.X., G.Z., J.P., D.C., Y.-J. Z. and L.W. wrote the paper with the help from all of the other coauthors. The manuscript was written through contributions of all authors. All authors have given approval to the final version of the manuscript.

Notes

The authors declare no competing financial interest.
All data needed to evaluate the conclusions in the paper are present in the paper and/or the Supporting Information. Additional data related to this paper may be requested from the authors.

■ ACKNOWLEDGMENTS

This research was performed in part at the RMIT Micro Nano Research Facility (MNRF) in the Victorian Node of the Australian National Fabrication Facility (ANFF) and the RMIT Microscopy and Microanalysis Facility (RMMF). This research was supported by the Australian Research Council Centre of Excellence in Future Low-Energy Electronics Technologies (CE170100039), the Natural Science Foundation of China (12074126), the National Key Research and Development Program of China (2016YFA0300404), the Fundamental Research Funds for the Central Universities (2020ZYGXZR076), the Collaborative Innovation Program of Hefei Science Center, CAS (Grant 2019HSC-CIP007), and the High Magnetic Field Laboratory of Anhui Province.

■ ABBREVIATIONS

vdW, van der Waals; F5GT, Fe_5GeTe_2; FM, ferromagnetism; AFM, antiferromagnetism; FGT, Fe_3GeTe_2; T_C, Curie temperature; EDLTs, electric double-layer transistors; SP-FET, solid proton field-effect transistor; MAE, magnetic anisotropic energy; DFT, density functional theory; PBE, Perdew−Burke−Ernzerhof; LDA+U, local density approximation plus Hubbard U; SOC, spin−orbit coupling

■ REFERENCES

(1) Ohno, H.; Chiba, A. D.; Matsukura, A. F.; Omiya, T.; Abe, E.; Dietl, T.; Ohno, Y.; Ohtani, K. Electric-field control of ferromagnetism. *Nature* **2000**, *408*, 944−946.

(2) Matsukura, F.; Tokura, Y.; Ohno, H. Control of magnetism by electric fields. *Nat. Nanotechnol.* **2015**, *10*, 209−220.

(3) Manipatruni, S.; Nikonov, D. E.; Young, I. A. Beyond CMOS computing with spin and polarization. *Nat. Phys.* **2018**, *14*, 338−343.

(4) Weisheit, M.; Fähler, S.; Marty, A.; Souche, Y.; Poinsignon, C.; Givord, D. Electric field-induced modification of magnetism in thin-film ferromagnets. *Science* **2007**, *315*, 349−351.

(5) Gong, C.; Li, L.; Li, Z.; Ji, H.; Stern, A.; Xia, Y.; Cao, T.; Bao, W.; Wang, C.; Wang, Y.; Qiu, Z. Q.; Cava, R. J.; Louie, S. G.; Xia, J.; Zhang, X. Discovery of intrinsic ferromagnetism in two-dimensional van der Waals crystals. *Nature* **2017**, *546*, 265−269.

(6) Huang, B.; Clark, G.; Navarro-Moratalla, E.; Klein, D. R.; Cheng, R.; Seyler, K. L.; Zhong, D.; Schmidgall, E.; McGuire, M. A.; Cobden, D. H.; Yao, W.; Xiao, D.; Jarillo-Herrero, P.; Xu, X. Layer-dependent ferromagnetism in a van der Waals crystal down to the monolayer limit. *Nature* **2017**, *546*, 270−273.

(7) Deng, Y.; Yu, Y.; Song, Y.; Zhang, J.; Wang, N. Z.; Sun, Z.; Yi, Y.; Wu, Y. Z.; Wu, S.; Zhu, J.; Wang, J.; Chen, X. H.; Zhang, Y. Gate-tunable room-temperature ferromagnetism in two-dimensional Fe_3GeTe_2. *Nature* **2018**, *563*, 94−99.

(8) Wang, Z.; Sapkota, D.; Taniguchi, T.; Watanabe, K.; Mandrus, D.; Morpurgo, A. F. Tunneling spin valves based on Fe_3GeTe_2/hBN/Fe_3GeTe_2 van der Waals heterostructures. *Nano Lett.* **2018**, *18*, 4303−4308.

(9) Wang, Z.; Gutiérrez-Lezama, I.; Ubrig, N.; Kroner, M.; Gibertini, M.; Taniguchi, T.; Watanabe, K.; Imamoğlu, A.; Giannini, E.; Morpurgo, A. F. Very large tunneling magnetoresistance in layered magnetic semiconductor CrI_3. *Nat. Commun.* **2018**, *9*, 1−8.

(10) Klein, D. R.; MacNeill, D.; Lado, J. L.; Soriano, D.; Navarro-Moratalla, E.; Watanabe, K.; Taniguchi, T.; Manni, S.; Canfield, P.; Fernández-Rossier, J.; Jarillo-Herrero, P. Probing magnetism in 2D van der Waals crystalline insulators via electron tunneling. *Science* **2018**, *360*, 1218−1222.

(11) Song, T.; Cai, X.; Tu, M. W.-Y.; Zhang, X.; Huang, B.; Wilson, N. P.; Seyler, K. L.; Zhu, L.; Taniguchi, T.; Watanabe, K.; McGuire, M. A.; Cobden, D. H.; Xiao, D.; Yao, W.; Xu, X. Giant tunneling magnetoresistance in spin-filter van der Waals heterostructures. *Science* **2018**, *360*, 1214−1218.

(12) Albarakati, S.; Tan, C.; Chen, Z.-J.; Partridge, J. G.; Zheng, G.; Farrar, L.; Mayes, E. L.; Field, M. R.; Lee, C.; Wang, Y.; Xiong, Y.; Tian, M.; Xiang, F.; Hamilton, A. R.; Tretiakov, O. A.; Culcer, D.; Zhao, Y.-J.; Wang, L. Antisymmetric magnetoresistance in van der Waals Fe_3GeTe_2/graphite/Fe_3GeTe_2 trilayer heterostructures. *Sci. Adv.* **2019**, *5*, No. eaaw0409.

(13) Wang, X.; Tang, J.; Xia, X.; He, C.; Zhang, J.; Liu, Y.; Wan, C.; Fang, C.; Guo, C.; Yang, W.; Guang, Y.; Zhang, X.; Xu, H.; Wei, J.; Liao, M.; Lu, X.; Feng, J.; Li, X.; Peng, Y.; Wei, H.; Yang, R.; Shi, D.; Zhang, X.; Han, Z.; Zhang, Z.; Zhang, G.; Yu, G.; Han, X. Current-driven magnetization switching in a van der Waals ferromagnet Fe_3GeTe_2. *Sci. Adv.* **2019**, *5*, No. eaaw8904.

(14) Dolui, K.; Petrovic, M. D.; Zollner, K.; Plechac, P.; Fabian, J.; Nikolic, B. K. Proximity spin-orbit torque on a two-dimensional magnet within van der Waals heterostructure: current-driven antiferromagnet-to-ferromagnet reversible nonequilibrium phase transition in bilayer CrI_3. *Nano Lett.* **2020**, *20*, 2288−2295.

(15) Jiang, S.; Shan, J.; Mak, K. F. Electric-field switching of two-dimensional van der Waals magnets. *Nat. Mater.* **2018**, *17*, 406−410.

(16) Wang, Z.; Zhang, T.; Ding, M.; Dong, B.; Li, Y.; Chen, M.; Li, X.; Huang, J.; Wang, H.; Zhao, X.; Li, Y.; Li, D.; Jia, C.; Sun, L.; Guo, H.; Ye, Y.; Sun, D.; Chen, Y.; Yang, T.; Zhang, J.; Ono, S.; Han, Z.; Zhang, Z. Electric-field control of magnetism in a few-layered van der Waals ferromagnetic semiconductor. *Nat. Nanotechnol.* **2018**, *13*, 554−559.

(17) Jiang, S.; Li, L.; Wang, Z.; Mak, K. F.; Shan, J. Controlling magnetism in 2D CrI_3 by electrostatic doping. *Nat. Nanotechnol.* **2018**, *13*, 549−553.

(18) Huang, B.; Clark, G.; Klein, D. R.; MacNeill, D.; Navarro-Moratalla, E.; Seyler, K. L.; Wilson, N.; McGuire, M. A.; Cobden, D. H.; Xiao, D.; Yao, W.; Jarillo-Herrero, P.; Xu, X. Electrical control of 2D magnetism in bilayer CrI_3. *Nat. Nanotechnol.* **2018**, *13*, 544−548.

(19) Yuan, H.; Shimotani, H.; Tsukazaki, A.; Ohtomo, A.; Kawasaki, M.; Iwasa, Y. High-density carrier accumulation in ZnO field-effect transistors gated by electric double layers of ionic liquids. *Adv. Funct. Mater.* **2009**, *19*, 1046−1053.

(20) May, A. F.; Ovchinnikov, D.; Zheng, Q.; Hermann, R.; Calder, S.; Huang, B.; Fei, Z.; Liu, Y.; Xu, X.; McGuire, M. A. Ferromagnetism near room temperature in the cleavable van der Waals crystal Fe_5GeTe_2. *ACS Nano* **2019**, *13*, 4436−4442.

(21) Ohta, T.; Sakai, K.; Taniguchi, H.; Driesen, B.; Okada, Y.; Kobayashi, K.; Niimi, Y. Enhancement of coercive field in atomically-thin quenched Fe_5GeTe_2. *Appl. Phys. Express* **2020**, *13*, 043005.

(22) May, A. F.; Bridges, C. A.; McGuire, M. A. Physical properties and thermal stability of $Fe_{5-x}GeTe_2$ single crystals. *Phys. Rev. Mater.* **2019**, *3*, 104401.

(23) Li, Z.; Xia, W.; Su, H.; Yu, Z.; Fu, Y.; Chen, L.; Wang, X.; Yu, N.; Zou, Z.; Guo, Y. Magnetic critical behavior of the van der Waals Fe_5GeTe_2 crystal with near room temperature ferromagnetism. *Sci. Rep.* **2020**, *10*, 1−10.

(24) Zhang, H.; Chen, R.; Zhai, K.; Chen, X.; Caretta, L.; Huang, X.; Chopdekar, R. V.; Cao, J.; Sun, J.; Yao, J.; Birgeneau, R.; Ramesh, R. Itinerant ferromagnetism in van der Waals $Fe_{5-x}GeTe_2$ crystals above room temperature. *Phys. Rev. B: Condens. Matter Mater. Phys.* **2020**, *102*, 064417.

(25) Fei, Z.; Huang, B.; Malinowski, P.; Wang, W.; Song, T.; Sanchez, J.; Yao, W.; Xiao, D.; Zhu, X.; May, A. F.; Wu, W.; Cobden, D. H.; Chu, J.-H.; Xu, X. Two-dimensional itinerant ferromagnetism in atomically thin Fe_3GeTe_2. *Nat. Mater.* **2018**, *17*, 778−782.

(26) Tan, C.; Lee, J.; Jung, S.-G.; Park, T.; Albarakati, S.; Partridge, J.; Field, M. R.; McCulloch, D. G.; Wang, L.; Lee, C. Hard magnetic properties in nanoflake van der Waals Fe_3GeTe_2. *Nat. Commun.* **2018**, *9*, 1−7.

(27) Zhang, Y.; Lu, H.; Zhu, X.; Tan, S.; Feng, W.; Liu, Q.; Zhang, W.; Chen, Q.; Liu, Y.; Luo, X.; Xie, D.; Luo, L.; Zhang, Z.; Lai, X. Emergence of Kondo lattice behavior in a van der Waals itinerant ferromagnet, Fe_3GeTe_2. *Sci. Adv.* **2018**, *4*, No. eaao6791.

(28) Kim, K.; Seo, J.; Lee, E.; Ko, K.-T.; Kim, B.; Jang, B. G.; Ok, J. M.; Lee, J.; Jo, Y. J.; Kang, W.; Shim, J. H.; Kim, C.; Yeom, H. W.; Min, B. I.; Yang, B.-J.; Kim, J. S. Large Anomalous Hall current induced by topological nodal lines in a ferromagnetic van der Waals semimetal. *Nat. Mater.* **2018**, *17*, 794−799.

(29) Zheng, G.; Xie, W.-Q.; Albarakati, S.; Algarni, M.; Tan, C.; Wang, Y.; Peng, J.; Partridge, J.; Farrar, L.; Yi, J.; Xiong, Y.; Tian, M.; Zhao, Y.-J.; Wang, L. Gate-tuned interlayer coupling in van der Waals ferromagnet Fe_3GeTe_2 nanoflakes. *Phys. Rev. Lett.* **2020**, *125*, 047202.

(30) Nagaosa, N.; Sinova, J.; Onoda, S.; MacDonald, A. H.; Ong, N. P. Anomalous Hall effect. *Rev. Mod. Phys.* **2010**, *82*, 1539.

(31) Seo, J.; Kim, D. Y.; An, E. S.; Kim, K.; Kim, G.-Y.; Hwang, S.-Y.; Kim, D. W.; Jang, B. G.; Kim, H.; Eom, G.; Seo, S. Y.; Stania, R.; Muntwiler, M.; Lee, J.; Watanabe, K.; Taniguchi, T.; Jo, Y. J.; Lee, J.; Min, B. I.; Jo, M. H.; Yeom, H. W.; Choi, S.-Y.; Shim, J. H.; Kim, J. S. Nearly room temperature ferromagnetism in a magnetic metal-rich van der Waals metal. *Sci. Adv.* **2020**, *6*, No. eaay8912.

https://doi.org/10.1021/acs.nanolett.1c01108
Nano Lett. 2021, 21, 5599−5605

(32) May, A. F.; Du, M.-H.; Cooper, V. R.; McGuire, M. A. Tuning magnetic order in the van der Waals metal Fe_5GeTe_2 by cobalt substitution. *Phys. Rev. Mater.* **2020**, *4*, 074008.

(33) Seo, J.; An, E. S.; Park, T.; Hwang, S.-Y.; Kim, G.-Y.; Song, K.; Noh, W.-s.; Kim, J. Y.; Choi, G. S.; Choi, M.; Oh, E.; Watanabe, K.; Taniguchi, T.; Park, J. -H.; Jo, Y. J.; Yeom, H. W.; Choi, S.-Y.; Shim, J. H.; Kim, J. S. Tunable high-temperature itinerant antiferromagnetism in a van der Waals magnet. *Nat. Commun.* **2021**, *12*, 2811.

(34) Tian, C.; Pan, F.; Xu, S.; Ai, K.; Xia, T.; Cheng, P. Tunable magnetic properties in van der Waals crystals $(Fe_{1-x}Co_x)_5GeTe_2$. *Appl. Phys. Lett.* **2020**, *116*, 202402.

(35) Nayak, A. K.; Fischer, J. E.; Sun, Y.; Yan, B.; Karel, J.; Komarek, A. C.; Shekhar, C.; Kumar, N.; Schnelle, W.; Kübler, J.; Felser, C.; Parkin, S. S. P. Large anomalous Hall effect driven by a nonvanishing Berry curvature in the noncolinear antiferromagnet Mn_3Ge. *Sci. Adv.* **2016**, *2*, No. e1501870.

(36) Blöchl, P. E. Projector augmented-wave method. *Phys. Rev. B: Condens. Matter Mater. Phys.* **1994**, *50*, 17953.

(37) Perdew, J. P.; Burke, K.; Ernzerhof, M. Generalized gradient approximation made simple. *Phys. Rev. Lett.* **1996**, *77*, 3865.

(38) Ferreira, L. G.; Marques, M.; Teles, L. K. Approximation to density functional theory for the calculation of band gaps of semiconductors. *Phys. Rev. B: Condens. Matter Mater. Phys.* **2008**, *78*, 125116.

(39) Tolba, S. A.; Gameel, K. M.; Ali, B. A.; Almossalami, H. A.; Allam, N. K. The DFT+U: Approaches, Accuracy, and Applications. In *Density Functional Calculations*; Yang, G., Ed.; IntechOpen: Rijeka, 2018, Chapter 1. DOI: 10.5772/intechopen.68548.

(40) Slater, J. C. Magnetic effects and the Hartree-Fock equation. *Phys. Rev.* **1951**, *82*, 538.

https://doi.org/10.1021/acs.nanolett.1c01108
Nano Lett. 2021, 21, 5599−5605